Korean J. Chem. Eng., 39(6), 1384-1395 (2022)
DOI: 10.1007/s11814-022-1075-6

pISSN: 0256-1115
eISSN: 1975-7220

Investigation on flow characteristic and reaction process inside an EVA autoclave reactor using CFD modeling combined with polymerization kinetics

Yiduo Wang*,, Cheng Liu*,**, Sheng Wang*,**, and He Dong*,**,†**

*Key Laboratory for Green Chemical Technology of the Ministry of Education, Tianjin University R&D Center for Petrochemical Technology, Tianjin 300072, China
**Collaborative Innovation Center of Chemical Science and Engineering, Tianjin 300072, China
(*Received 15 October 2021 • Revised 20 January 2022 • Accepted 23 January 2022*)

Abstract−EVA is an important high-performance resin material obtained by the copolymerization of ethylene and vinyl acetate. In the present study, a comprehensive computational fluid dynamics (CFD) model was established to study the EVA free radical copolymerization process. The polymerization kinetic model was combined with the CFD model. The EVA copolymerization reaction mechanism was verified by comparing the simulation results with the experimental results. Detailed information of the flow field inside the industrial EVA autoclave reactor was obtained. With the increase of the impeller speed, both the axial and radial flows inside the autoclave reactor were enhanced. The high impeller speed improved the fluid mixing and the homogeneity of temperature distribution. The increase of the impeller speed improved the initiator dispersion near the inlets, thereby increasing the efficiency of the initiator. The influence of operating conditions on monomer conversion and specific initiator consumption per 1% of the monomer reacted was investigated. The simulation results give deep insight into the free radical copolymerization process inside the autoclave reactor and supply the guidelines for developing an industrial autoclave reactor.

Keywords: EVA, Free Radical Polymerization, CFD, Autoclave, Operating Conditions

INTRODUCTION

Ethylene-vinyl acetate copolymer (EVA) is obtained by the copolymerization of ethylene monomer and vinyl acetate (VA) monomer. EVA resins, the EVA copolymer with a VA content of 5-40%, are widely used to modify polyolefin resins, oil additives, wire sheathings, films, and hot melt adhesives [1,2]. The industrial production of EVA resin adopts a free radical high-pressure copolymerization process that is derived from the low-density polyethylene (LDPE) process. Usually, the reaction temperature is controlled at 150-300 °C, and the reaction pressure is kept at 100-300 MPa. EVA copolymerization is an exothermic reaction. The polymerization heat of ethylene and vinyl acetate is 95 kJ/mol and 145 kJ/mol, respectively [3]. Since the EVA polymerization reaction is carried out under very high pressure, the reactor wall is usually thick. Compared with the heat of polymerization, the heat removed from the reactor wall is small. Thus, the reactor can be considered adiabatic. When the reaction temperature is above 300 °C, ethylene decomposition reactions can be triggered, which will cause the thermal runaway of the reactor. EVA free radical high-pressure copolymerization is usually carried out in autoclave and tubular reactors. The height-to-diameter ratio of the autoclave reactor is usually in the range of 5 : 1-20 : 1. There are multiple feed inlets along the axial direction of the autoclave reactor [4-7]. The polymerization process is closely related to the complex flow, temperature, and concentration field distribution inside the autoclave reactor. Studying the polymerization process inside the EVA autoclave reactor has important guiding significance for the design of the reactor and the optimization of operating conditions.

The reaction process is closely related to mixing. If the mixing is poor, the monomers and initiators will not be well dispersed, which may cause violent reactions in partial zones [4,7,8]. In addition, the specific initiator consumption per 1% of the monomer reacted is closely related to the mixing. In the EVA polymerization reaction, the initiator is not recyclable, so the specific initiator consumption per mass of the monomer reacted is an important indicator to evaluate the economic efficiency of EVA industrial production. The industry usually enhances mixing by increasing the impeller speed. The effects of impeller speed on polymerization stirred reactors have been reported by several articles [8-10]. Increasing the impeller speed is often beneficial to improving the homogeneity of the reaction mixture inside the reactor. However, the influence of impeller speed on EVA polymerization autoclave reactor is not evident. It is necessary to study the influence of impeller speed on the flow field distribution, temperature field distribution, concentration field distribution, and polymerization process inside the EVA autoclave reactor. In addition to mixing, the inlet temperature and the initiator concentration also significantly influence the polymerization process [11].

Luft et al. [12] investigated the effect of the addition of triethylaluminum on the copolymerization of ethylene and vinyl acetate initiated by tert-butyl perpivalate (TBPPI). They found an increase in conversion and a decrease in peroxide consumption after the addition of triethylaluminum. However, their studies cannot reflect the

†To whom correspondence should be addressed.
E-mail: donghe@tju.edu.cn

actual operating status of polymerization reactors under industrial conditions and obtain information of the flow field. To describe the operating status of industrial polymerization reactors, some free radical high-pressure copolymerization models of EVA and LDPE autoclave reactors have been reported [3,7,13-15]. These models usually assumed that the EVA autoclave reactors were composed of multiple fully mixed continuous stirred tank reactors (CSTR) connected in series, which cannot reflect the flow field information of the reactor. Since the reactors have been simplified, these models are only applicable to specific factory conditions. However, the non-ideal flow inside the EVA autoclave reactor is closely related to the reaction process, affecting the distribution of temperature field and concentration field and significantly impacting the polymerization rate and monomer conversion. The computational fluid dynamics (CFD) method can replace time-consuming and expensive experimental operations to obtain detailed flow field information. CFD simulations of the polymerization reactors have been reported [8-10,16,17]. By combining the polymerization reaction kinetics model with the CFD model, information on the distribution of flow field, temperature field, and concentration field can be obtained. However, these studies usually focus on the effects of operating conditions on the reaction process and rarely discuss the mixing mode of the reactor and its effect on polymerization. In addition, these studies only consider the polymerization of one monomer and do not consider the copolymerization between different monomers.

This work established a comprehensive model of the EVA autoclave reactor. The EVA free radical copolymerization process was simulated by combining the CFD and polymerization kinetic models. The effects of impeller speed on flow field distribution were investigated, and the influence of autoclave reactor mixing mode on the EVA polymerization process was discussed. The effects of operating conditions (impeller speed, inlet temperature, and initiator concentration) on the EVA polymerization process were studied.

MATHEMATICAL MODEL

1. CFD Model

A three-dimensional steady-state model was used to simulate the single-phase flow in the EVA autoclave reactor. The continuity, momentum balance, energy conservation, and species transport equations are as follows [18,19]:

Continuity equation,

$$\frac{\partial \rho}{\partial t}+\frac{\partial(\rho u_i)}{\partial x_i}=0 \tag{1}$$

where ρ is the density, u_i is the velocity components, t is the time, and x_i is the Cartesian coordinate.

As the flow behavior is highly unsteady at high Reynolds numbers, the Reynolds-averaged turbulence approximation was adopted to model such flow configurations. The momentum balance equation is as follows:

$$\frac{\partial(\rho \bar{u}_i)}{\partial t}+\frac{\partial}{\partial x_j}(\rho \bar{u}_i \bar{u}_j+\overline{\rho u_i' u_j'})+\frac{\partial \bar{p}}{\partial x_i}+\frac{\partial \bar{\tau}_{ij}}{\partial x_j}=\rho g_i \tag{2}$$

$$\tau_{ij}=-\mu\left(\frac{\partial u_i}{\partial x_j}+\frac{\partial u_j}{\partial x_i}-\frac{2}{3}\delta_{ij}\frac{\partial u_k}{\partial x_k}\right) \tag{3}$$

where $\bar{u}_i$ is the mean velocity components, u_i' is the fluctuating velocity components, $\bar{p}$ is the mean pressure, τ_{ij} is the stress tensor, μ is the dynamic viscosity, δ_{ij} is the Kronecker delta, and $(\overline{\rho u_j' u_i'})$ is the Reynolds stress. To correctly account for turbulence, Reynolds stresses are modelled by the realizable k-ε (RKE) model. Governing equations for turbulent kinetic energy k and kinetic energy dissipation rate ε are [20]:

$$\frac{\partial}{\partial t}(\rho k)+\frac{\partial}{\partial x_i}(\rho u_i k)=\frac{\partial}{\partial x_j}\left[\left(\mu+\frac{\mu_t}{\sigma_k}\right)\frac{\partial k}{\partial x_j}\right]+\mu_t\left(\frac{\partial u_i}{\partial x_j}+\frac{\partial u_j}{\partial x_i}\right)\frac{\partial u_i}{\partial x_j}-\rho\varepsilon \tag{4}$$

$$\frac{\partial}{\partial t}(\rho \varepsilon)+\frac{\partial}{\partial x_i}(\rho u_i \varepsilon)=\frac{\partial}{\partial x_j}\left[\left(\mu+\frac{\mu_t}{\sigma_\varepsilon}\right)\frac{\partial \varepsilon}{\partial x_j}\right]+\rho C_1 S\varepsilon-\rho C_2\frac{\varepsilon^2}{k+\sqrt{\upsilon\varepsilon}} \tag{5}$$

in which, μ_t is the turbulent viscosity,

$$\mu_t=\rho C_\mu\frac{k^2}{\varepsilon} \tag{6}$$

$C_1=\max\left[0.43;\ \frac{\eta}{\eta+5}\right]$, $C_2=1.9$, $C_\mu=0.09$, $\sigma_k=1.0$, $\sigma_\varepsilon=1.2$, $\eta=\frac{Sk}{\varepsilon}$, $S=\sqrt{2S_{ij}\cdot S_{ij}}$, $S_{ij}=\frac{1}{2}\left(\frac{\partial u_i}{\partial x_j}+\frac{\partial u_j}{\partial x_i}\right)$.

Energy conservation equation:

$$\frac{\partial(\rho e)}{\partial t}+\frac{\partial}{\partial x_i}[u_i(\rho e+p)]=\frac{\partial}{\partial x_i}\left[k_{eff}\frac{\partial T}{\partial x_i}-\sum_m h_m J_{m,i}+u_j\tau_{ij}\right]+S_h \tag{7}$$

$$e=h+\frac{p}{\rho}+\frac{u_i^2}{2} \tag{8}$$

where e is the total energy, h is the specific enthalpy, k_{eff} is the effective thermal conductivity, $J_{m,i}$ is the diffusion flux of component m, and S_h is the source term.

Species transport equation:

$$\frac{\partial(\rho Y_m)}{\partial t}+\frac{\partial(\rho u_i Y_m)}{\partial x_i}=-\frac{\partial J_{m,i}}{\partial x_i}+S_m \tag{9}$$

where Y_m and S_m are the mass fraction and reaction source of component m.

$$J_{m,i}=-\left(\rho D_{m,i}+\frac{\mu_t}{Sc_t}\right)\nabla Y_m \tag{10}$$

where $D_{m,i}$ is the diffusion coefficient of component m, Sc_t is the Schmidt number.

$$Sc_t=\frac{\mu_t}{\rho D_t} \tag{11}$$

2. Polymerization Kinetic Model

The high-pressure copolymerization of EVA follows the free radical polymerization mechanism. In this study, tert-butyl peroxy-2-ethylhexanoate (TBPO) was used as the initiator, and n-butane was used as the modifier. In addition, TBPPI initiator was used in the copolymerization mechanism model verification. The free radicals generated by the initiator decomposition cannot be consumed entirely to initiate the polymerization reaction. Some free radicals may participate in side reactions. Becker et al. [21] investigated the initiator efficiency f of different initiators, where f_{TBPO} is 0.5-0.7 and f_{TBPPI} is 0.3-0.5. In this study, f_{TBPO} adopted was 0.7 and f_{TBPPI} adopted

Table 1. EVA copolymerization reaction mechanism

Elementary reaction	Mechanism	Pseudo-kinetic rate constants
Initiator decomposition	$I_l \xrightarrow{k_{dl}} 2R_0 (l=1, 2 \ldots N_I)$	
Initiation	$R_0 + M \xrightarrow{k_{in}} R_1$	$k_{in} = \sum_{j=1}^{2} k_{inj} f_j$
Propagation	$R_n + M \xrightarrow{k_p} R_{n+1}$	$k_p = \sum_{i=1}^{2}\sum_{j=1}^{2} k_{pij} \varphi_i f_j$
Termination by combination	$R_m + R_n \xrightarrow{k_{tc}} P_{m+n}$	$k_{tc} = \sum_{i=1}^{2}\sum_{j=1}^{2} k_{tcij} \varphi_i \varphi_j$
Termination by disproportionation	$R_m + R_n \xrightarrow{k_{td}} P_m + P_n$	$k_{td} = \sum_{i=1}^{2}\sum_{j=1}^{2} k_{tdij} \varphi_i \varphi_j$
Chain transfer to monomer	$R_n + M \xrightarrow{k_{tm}} R_1 + P_n$	$k_{tm} = \sum_{i=1}^{2}\sum_{j=1}^{2} k_{tmij} \varphi_i f_j$
Chain transfer to polymer	$R_n + P_m \xrightarrow{k_{tp}} R_m + P_n$	$k_{tp} = \sum_{i=1}^{2}\sum_{j=1}^{2} k_{tpij} \varphi_i F_j$
Chain transfer to modifier	$R_n + A \xrightarrow{k_{ta}} R_1 + P_n$	$k_{ta} = \sum_{j=1}^{2} k_{tai} \varphi_i$
β-Scission of internal radicals	$R_n + P_m \xrightarrow{k_\beta} R_z + P_n + P_{m-z}$	$k_\beta = \sum_{i=1}^{2}\sum_{j=1}^{2} k_{\beta ij} \varphi_i F_j$

was 0.35. The elementary reactions considered in this study include initiator decomposition, initiation, propagation, chain transfer to monomer, chain transfer to polymer, chain transfer to modifier, termination by combination, termination by disproportionation, and β-scission of internal radicals [3,17]. To simplify the calculation of the copolymerization reaction, Xie et al. [22-24] proposed the pseudo-kinetic rate constant method. The elementary reactions and the pseudo-kinetic rate constants of the ethylene-VA binary copolymerization are shown in Table 1.

f_i is the mole fraction of monomer *i* in monomer mixture,

$$f_1 = \frac{M_1}{M_1 + M_2} \tag{12}$$

$$f_2 = 1 - f_1 \tag{13}$$

φ_i is the mole fraction of radical *i*, which can be derived from the assumption of the long chain approximation [25,26],

$$k_{pij} \varphi_i f_j = k_{pji} \varphi_j f_i \tag{14}$$

$$\varphi_1 = \frac{k_{p21} f_1}{k_{p21} f_1 + k_{p12} f_2} \tag{15}$$

$$\varphi_2 = 1 - \varphi_1 \tag{16}$$

F_i is the mole fraction of monomer *i* in polymer [3],

$$F_1 = \frac{(r_1 - 1) f_1^2 + f_1}{(r_1 + r_2 - 2) f_1^2 + 2(1 - r_2) f_1 + r_2} \tag{17}$$

$$F_2 = 1 - F_1 \tag{18}$$

where r_1, r_2 are reactivity ratios.

3. Moment Method

Since the active polymer chain and the dead polymer chain have an infinite number of chain lengths, the moment method is used to simplify the differential equations to realize the calculation of the copolymer chain length distributions [3,7,27].

The zero moment, first moment, and second moment equations of the active polymer chain are as follows:

$$\lambda_i = \sum_{n=1}^{\infty} n^i [R_n] \tag{19}$$

The zero moment, first moment, and second moment equations of the dead polymer chain are as follows:

$$\mu_i = \sum_{n=2}^{\infty} n^i [P_n] \tag{20}$$

The final moment rate equations are as follows: (the detailed derivation process is given in the Supplemental files):

$$r_{\lambda_0} = 2 f k_d [I] - (k_{tc} + k_{td}) \lambda_0^2 \tag{21}$$

$$r_{\lambda_1} = 2 f k_d [I] - (k_{tm}[M] + k_{ta}[A]) \lambda_1 + k_p [M] \lambda_0 + k_{tp} (\mu_2 \lambda_0 - \mu_1 \lambda_1) - (k_{tc} + k_{td}) \lambda_0 \lambda_1 + k_\beta \left(\frac{1}{2} \mu_2 \lambda_0 - \mu_1 \lambda_1 \right) \tag{22}$$

$$r_{\lambda_2} = 2 f k_d [I] - (k_{tm}[M] + k_{ta}[A]) \lambda_2 + 2 k_p [M] \lambda_1 + k_{tp} (\mu_3 \lambda_0 - \mu_1 \lambda_2) - (k_{tc} + k_{td}) \lambda_0 \lambda_2 + k_\beta \left(\frac{1}{3} \mu_3 \lambda_0 - \frac{1}{2} \mu_2 \lambda_0 + \frac{1}{6} \mu_1 \lambda_0 - \mu_1 \lambda_2 \right) \tag{23}$$

$$r_{\mu_0} = (k_{tm}[M] + k_{td}[A]) \lambda_0 + \left(\frac{1}{2} k_{tc} + k_{td} \right) \lambda_0^2 + k_\beta \lambda_0 \mu_1 \tag{24}$$

$$r_{\mu_1} = (k_{tm}[M] + k_{ta}[A]) \lambda_1 - k_{tp} (\mu_2 \lambda_0 - \mu_1 \lambda_1) + (k_{td} + k_{tc}) \lambda_0 \lambda_1 + k_\beta \left(\lambda_1 \mu_1 - \frac{1}{2} \lambda_0 \mu_0 \right) \tag{25}$$

$$r_{\mu_2} = (k_{tm}[M] + k_{ta}[A]) \lambda_2 - k_{tp} (\mu_3 \lambda_0 - \mu_1 \lambda_2) + (k_{td} + k_{tc}) \lambda_0 \lambda_2 + k_{tc} \lambda_1^2 \tag{26}$$

$$+k_{\beta}\left[\lambda_2\mu_2-\lambda_0\left(\frac{2}{3}\mu_3+\frac{1}{2}\mu_2-\frac{1}{6}\mu_1\right)\right]$$

In this study, the Hulburt and Katz approximation [28] was used to break the dependence of the n order polymer moment equation on the n+1 order polymer moment equation when considering the chain transfer to the polymer reaction. In the above equation, μ_3 can be expressed as:

$$\mu_3=\frac{\mu_2}{\mu_1\mu_0}(2\mu_2\mu_0-\mu_1^2) \tag{27}$$

CFD SIMULATION

The industrial-scale EVA autoclave reactor is designed based on a factory's high-pressure polyethylene process. The process adopts the mode of double autoclave reactors in series. Each autoclave reactor has a volume of 0.75 m^3 and can produce 60,000 tons of LDPE per year. In this study, an industrial EVA autoclave reactor was established with a volume of 0.75 m^3, consisting of a cylinder and two standard elliptical heads. The reactor contains four inlets. The 45° pitched-blade turbines were used to realize the mixing of feed. To achieve a good dispersion of the initiator, the impellers below inlet 2, inlet 3 and inlet 4 were replaced with Rushton impellers. The structures of the reactor and impellers are shown in Fig. 1(a) and the parameters are shown in Table 2.

The CFD software package STAR-CCM+ was used for simulation. The reactor was divided into the stationary and rotating zones near the impeller. The overlapping surfaces between the stationary and rotating zones were set as the interface. Unstructured polyhedral cells and prismatic layer cells were used to discretize the three-dimensional computing area. To accurately capture the flow details near the impeller and the interface, the impeller and interface cells were refined. The unstructured grids of the computational domain are shown in Fig. 1(b). The grid independence test is shown in Fig. 2. The monomer conversion and the average velocity of the reactor axis section are basically stable after the grid number reaches more than 3 million. Considering the calculation accuracy and time factors, the final three-dimensional model had 3166905 cells. The multiple reference frame (MRF) method was used to describe the rotation of the impeller [29]. The SIMPLE algorithm was used to solve the pressure-velocity coupling, and the discretization of the transport equation adopts the second-order upwind scheme. In the steady-state simulation of the EVA polymerization reaction, the turbulence model adopted the realizable k-ε (RKE) model. The polymerization reaction model was activated, the governing equations and energy equations of each component were solved to obtain the temperature distribution, the concentration distribution of each component, and the molecular weight of the copolymer. Simultaneously, the viscosity model was combined to obtain the viscosity distribution inside the reactor. Convergence was achieved when

Table 2. Reactor structure parameters

Reactor structure parameters		Value (mm)
Diameter of cylinder		450
Height of cylinder		4,500
The long axis of the standard elliptical head		225
The short axis of the standard elliptical head		1,12.5
Inlet and outlet positions	Inlet 1	4,725
	Inlet 2	4,212.5
	Inlet 3	2,812.5
	Inlet 4	1,412.5
	Outlet	−112.5
Diameter of inlet and outlet		20
Diameter of shaft		60
Diameter of impeller		430
Thickness of impeller		6
Width of impeller		45

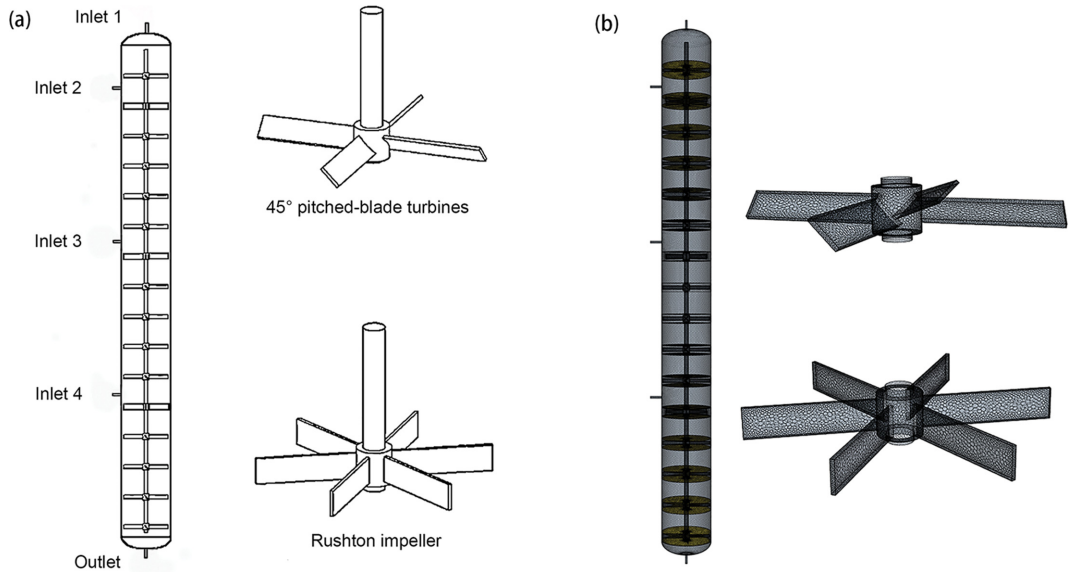

Fig. 1. (a) Schematic geometry, and (b) Grid geometry of EVA autoclave reactor and impeller.

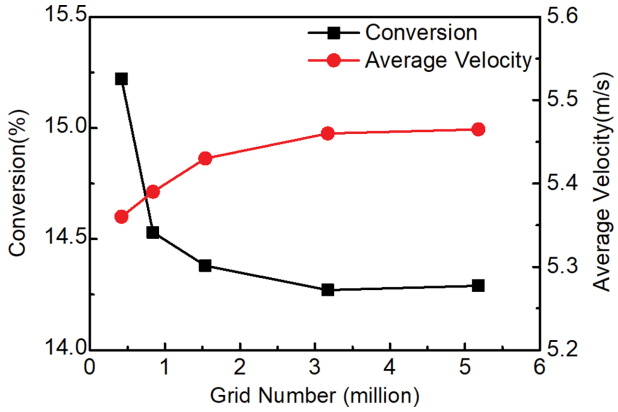

Fig. 2. Grid independence test.

the temperature and composition at the outlet did not change with the number of iterations. All equations were solved in steady-state mode, and convergence was reached after 40000 iterations. Each simulation was run parallel on 48 CPUs and converged within 45.84 hours.

The reactor was adiabatic. Pladis et al. [5] compared the effects of pure initiator feed and initiator mixed with ethylene feed of the LDPE polymerization reaction. The results showed that the pure initiator feed tends to cause local overheating of the autoclave reactor and trigger the ethylene decomposition reaction. Therefore, the premixed of initiator and monomer was used in this study used. In the factory's high-pressure polyethylene process, the ethylene monomer coming from the compression section is divided into four streams. Three streams (each accounting for 1/4 of the total) enter the first reactor's upper, middle, and lower positions. The other stream is equally divided into two streams (each accounting for 1/8 of the total) and enters the top motor chambers of the two reactors to cool the motors directly. So in this study, the ratio of inlet flow rates of monomer, initiator, and modifier at the four inlets was inlet 1 : inlet 2 : inlet 3 : inlet 4=1 : 2 : 2 : 2. The operating conditions and physical parameters are shown in Table 3. Since the concentration of TBPO and n-butane is relatively small, the specific heat capacity and heat of polymerization of TBPO and n-butane (CTA) were ignored. Since the changes are small because of low monomer conversion, the density of the fluid was assumed to be constant [7]. Since the VA concentration of the EVA polymerization process simulated in this study was low, about 20%, the mixture's viscosity was assumed to be equivalent to the LDPE polymerization process. The following viscosity model was used in our research [6]:

$$\eta_m = \eta_{ethy}\exp\left[2.00+0.017\left(\frac{\mu_1}{\mu_0}\right)^{0.556}\mu_1+\frac{E_v}{R_g}\left(\frac{1}{T}-\frac{1}{423}\right)\right] \quad (28)$$

in which, η_{ethy} is the viscosity of ethylene.

$$E_v = -500+560\mu_1 \ \text{kcal/(kg·mol)} \quad (29)$$

The kinetic rate constants during high-pressure polymerization were obtained from the Arrhenius equation [30]:

$$k = k_0\exp\left[-\left(\frac{E_a+p\Delta V}{RT}\right)\right] \quad (30)$$

where k_0 is the frequency factor, E is the activation energy, and ΔV is the activation volume. The kinetic rate constant values of each elementary reaction used in this study are shown in Table 4.

RESULTS AND DISCUSSION

1. Mechanism Model Verification

To verify the EVA copolymerization mechanism in Sections 2 and 3, we first simulated the laboratory-scale EVA copolymerization reactor and compared the simulation results with the experimental results.

Table 3. Operating conditions and physical parameters

Parameters	Value
Residence time (s)	40
Feed mass ratio (ethylene : VA)	8 : 2
TBPO (ppm)	30-75
n-butane (ppm)	900
Inlet temperature (K)	383-413
Pressure (MPa)	170
Impeller speed (rpm)	100-900
Density [7] (kg·m^{-3})	520
Specific heat [3] (J·kg^{-1}·K^{-1})	
Ethylene	1,569.7+6.58×(T−273.15)
Polyethylene	1,964.6
VA	5,298.5+3.47×(T−273.15)
Polyvinylacetate	1,343.5+3.99×(T−273.15)
Thermal conductivity of mixture [17] (J·kg^{-1}·K^{-1})	0.1998
Heat of polymerization [3] (kJ·mol^{-1})	
Ethylene	95
VA	142.76

Table 4. Kinetic rate constants of ethylene and VA polymerization

	Elementary reaction	Symbol	k_0* ($L \cdot mol^{-1} \cdot s^{-1}$)	E ($J \cdot mol^{-1}$)	ΔV ($cm^3 \cdot mol^{-1}$)
TBPPI [6]	Initiator decomposition	k_d	7.95×10^{13}	117,140	3.45
TBPO [6]	Initiator decomposition	k_d	5.75×10^{11}	109,148	6.11
Ethylene [27]	Initiation	k_{in}	1.25×10^{8}	33,767	−19.7
	Propagation	k_p	1.25×10^{8}	33,767	−19.7
	Termination by combination	k_{tc}	1.25×10^{9}	4,184	13
	Termination by disproportionation	k_{td}	1.25×10^{9}	4,184	13
	Chain transfer to monomer	k_{tm}	1.25×10^{5}	33,767	−19.7
	Chain transfer to polymer	k_{tp}	4.38×10^{8}	54,936	4.4
	Chain transfer to modifier	k_{ta}	2.62×10^{7}	49,664	−19.5
	β-scission of internal radicals	k_β	1.292×10^{7}	47,149	−16.8
VA [30]	Initiation	k_{in}	3.2×10^{7}	26,334	
	Propagation	k_p	3.2×10^{7}	26,334	
	Termination by combination	k_{tc}	3.7×10^{9}	13,376	
	Termination by disproportionation	k_{td}	3.7×10^{9}	13,376	
	Chain transfer to monomer	k_{tm}	7.616×10^{3}	26,334	
	Chain transfer to polymer	k_{tp}	1.088×10^{4}	26,334	
Reactivity ratios [7]	Ethylene (1)		$r_1\left(\frac{k_{p11}}{k_{p12}}\right)$	1.06	
	VA (2)		$r_2\left(\frac{k_{p22}}{k_{p21}}\right)$	1.09	

*When the reaction is the first order, the unit of k_0 is s^{-1}; when the reaction is the second order, the unit of k_0 is $L \cdot mol^{-1} \cdot s^{-1}$.

Table 5. The comparison of simulation and experimental system with the TBPPI initiator

VA concentration (wt%)	Conversion (%)			Initiator consumption (g/kg polymer)		
	Experiment [12]	Simulation	Error	Experiment [12]	Simulation	Error
13	13.9	15.1	8.6	2.24	1.87	−16.5
36	17.8	15.9	−10.7	1.3	1.46	−12.3

Table 5 shows the comparison of simulation and experimental system with the TBPPI concentration of 50 mole ppm, the pressure of 190 MPa, the temperature of 150 °C, and residence of 40 s. For the VA concentrations of 13 wt% and 36 wt%, the errors of CFD simulations of EVA polymerization conversion and initiator consumption are both within 20%.

2. Simulation Results

The EVA autoclave reactor was simulated with the inlet temperature of 403 K and the initiator concentration of 30 ppm. Fig. 3(a) and Fig. 3(b) show the distribution contours of temperature, monomer mass fraction, EVA mass fraction, viscosity, and initiator concentration of the axial section of the reactor at impeller speeds of 100 rpm and 700 rpm, respectively. The reactor was divided into three reaction zones. The cold streams from inlets were quickly heated, and the reaction temperature raised continuously along the axis direction in each reaction zone. The initiator decomposed quickly after injection. The primary free radicals generated by the initiator decomposition can further initiate polymerization. As the monomers were consumed, the EVA mass fraction increased along the axial direction in each reaction zone. The viscosity distribution shows the same trend as the EVA concentration distribution. In Fig. 3(a), when the impeller speed was 100 rpm, the temperature and EVA mass fraction near the stirring shaft were significantly higher than the wall surface due to poor mixing near the stirring shaft. In Fig. 3(b), when the impeller speed was increased to 700 rpm, the radial distribution gradient of temperature and EVA mass fraction were significantly reduced.

3. Influence of Impeller Speed

The influence of impeller speed on flow characteristics was investigated. Fig. 4 is the velocity distribution vector diagram between two adjacent 45° pitched-blade turbines of the reactor axial-section at the impeller speed from 100 rpm to 900 rpm. Two upward and downward streams are formed at the tip of the impeller, where the upward stream produced by the lower impeller and the downward stream produced by the upper impeller converge in the middle of the two adjacent impellers and flow together to the next reaction zone. In addition to the axial flow, radial flow was also formed between the wall and the stirring shaft. The increase of the impeller speed enhanced the axial and radial flow.

Fig. 5 is the velocity distribution streamline diagram of the reactor shaft section (z/H=0.65-0.82, z is the observation position, H is the height of the reactor) of different impeller speeds. The fluid

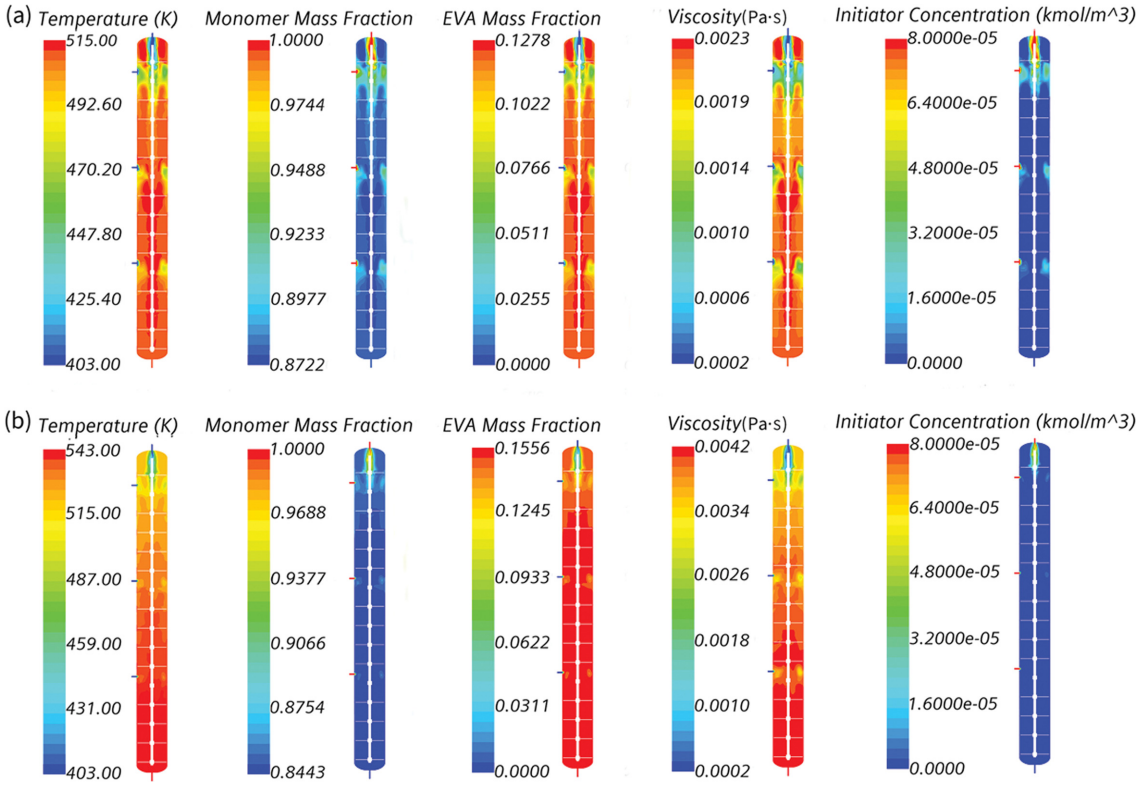

Fig. 3. Contours of temperature, initiator mass fraction, monomer mass fraction, EVA mass fraction, and viscosity at the reactor axial-section: (a) 100 rpm; (b) 700 rpm.

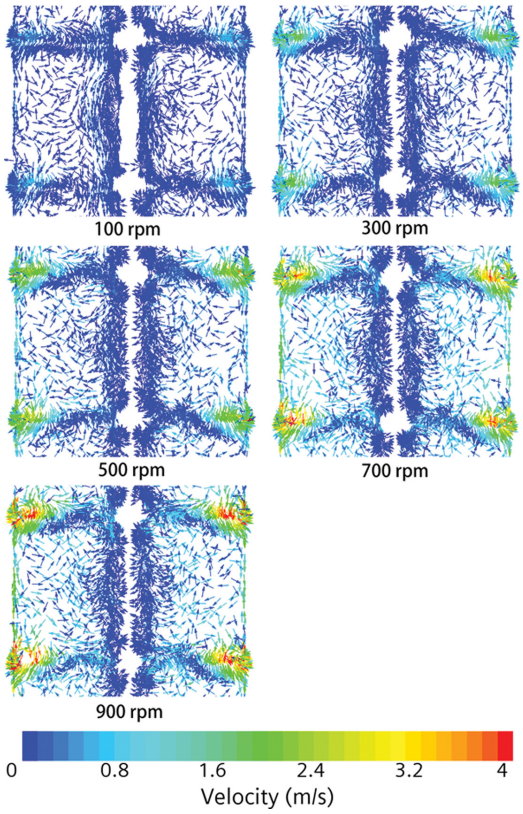

Fig. 4. Velocity distribution vector diagram between two impellers with different impeller speeds.

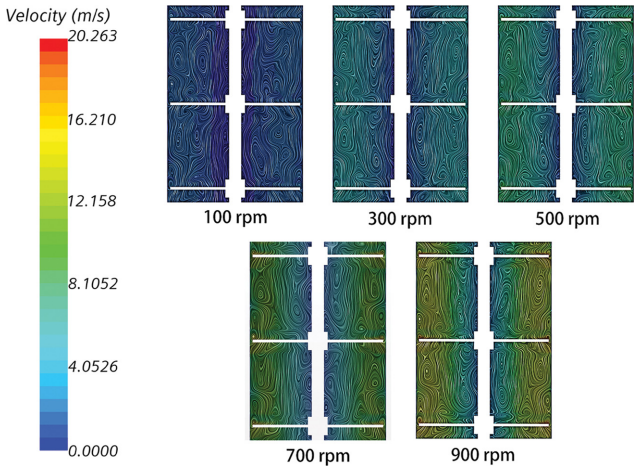

Fig. 5. Velocity distribution streamline diagram with different impeller speeds.

flow route changed with the impeller speed increased. When the impeller speed was 100 rpm, eddies were mainly formed away from the shaft and the axial flow was formed near the stirring shaft. Eddies gradually appeared near the shaft as the impeller speed increased to 500 rpm, indicating that the mixing at the shaft improved, and the fluid at the main body of the flow and the shaft could be fully mixed at this time. After reaching 700 rpm and 900 rpm, the flow pattern no longer changed significantly with the increase of the impeller speed, but the axial and radial velocities were greatly im-

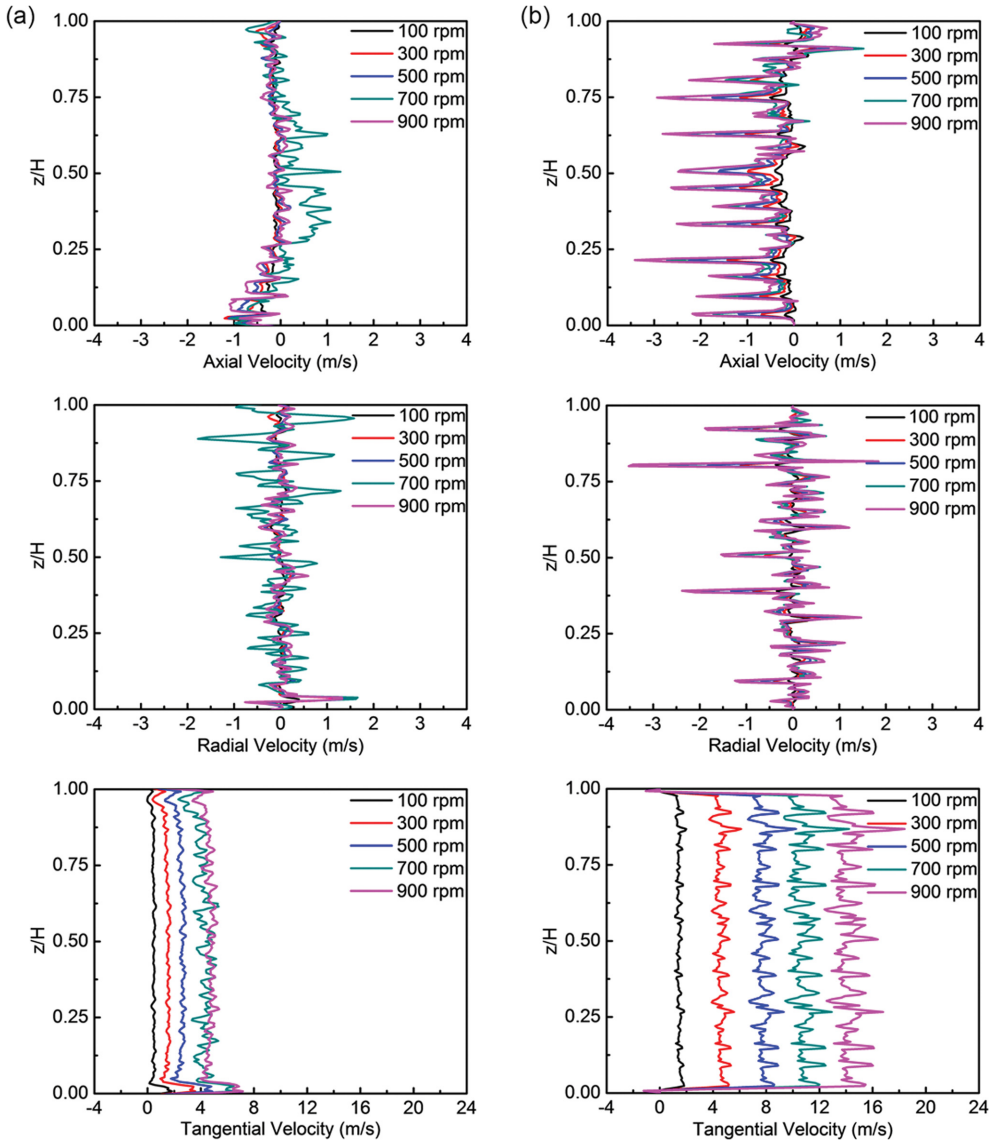

Fig. 6. The distribution of the axial, radial and tangential velocities at (a) r=0.05 m and (b) r=0.2 m.

proved.

To further quantitatively investigate the velocity distribution in the reactor at different impeller speeds, the velocities at r=0.05 m (near the stirring shaft) and r=0.2 m (near the wall) were compared. The distribution of the axial, radial and tangential velocity components are shown in Fig. 6. The three velocity components near the wall were larger than the stirring shaft. It indicates that the mixing near the wall was better than the mixing near the stirring shaft. When the impeller speed was 100 rpm, the two observation positions' axial velocity and radial velocity were close to 0 m/s. The tangential flow was mainly generated in the reactor. However, tangential flow is not helpful for the mixing in the reactor. With the impeller speed increased from 100 rpm to 700 rpm, the two observation positions' axial velocity and radial velocity had greatly improved, and the maximum radial velocity near the stirring shaft reached 2 m/s. As the impeller speed increased to 900 rpm, the maximum tangential velocity increased to about 20 m/s, but the axial and radial velocity did not increase further. Moreover, the axial and radial velocity significantly decreased near the stirring shaft. The decrease of axial and radial velocity is attributed to the large tangential flow inertia generated in the reactor, weakening the axial and radial flow near the stirring shaft.

To investigate the influence of impeller speed on the polymerization process, the EVA autoclave reactor with different impeller speeds at an inlet temperature of 403 K and initiator concentration of 30 ppm was simulated. Fig. 7 shows the contours of the unreacted initiator concentration near the inlet at different impeller speeds. There is a high concentration of unreacted initiator near the inlet at the impeller speeds of 100 and 300 rpm. The reactor had a large initiator concentration gradient from the area near the inlet to the main body area. It shows that the fluid mixing was poor at the lower impeller speeds of 100 and 300 rpm. As the impeller speed increased to 500, 700, 900 rpm, the mixing was improved and the initiator concentration gradient dropped.

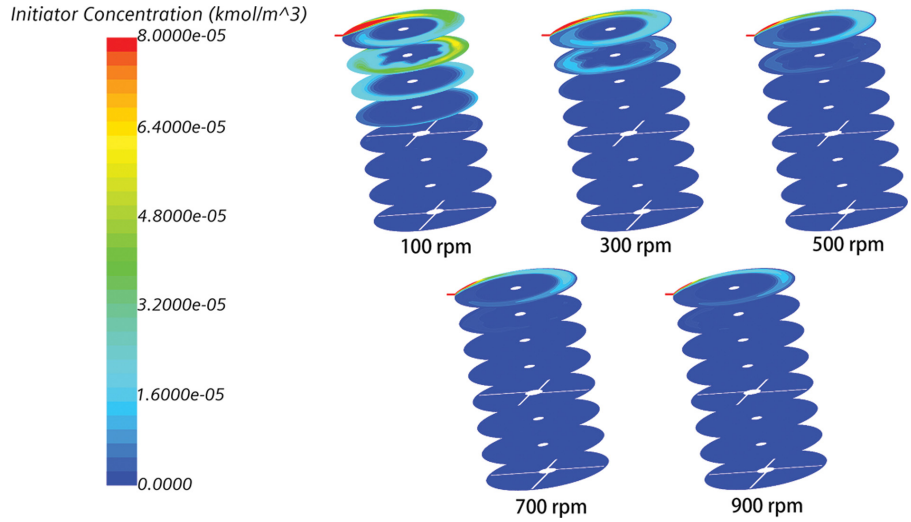

Fig. 7. Contours of initiator mass fraction at the reactor cross-sections near inlet 3 with different impeller speeds.

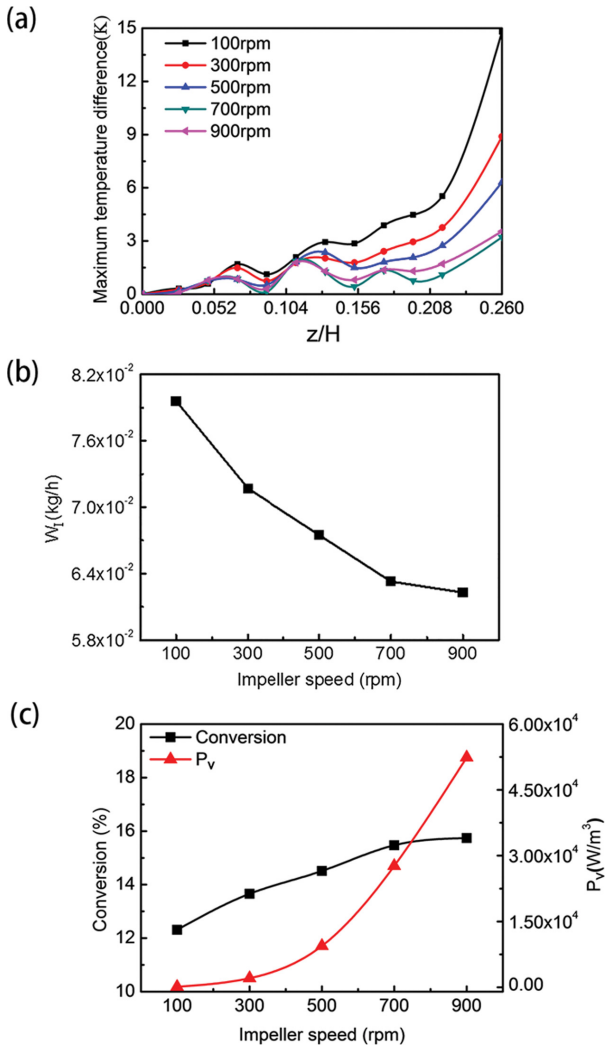

Fig. 8. (a) The maximum temperature difference of the reactor cross-sections at different heights (z/H=0-0.26) with the impeller speed from 100 rpm to 900 rpm; The effects of impeller speed on (b) W_I, (c) P_VT and the outlet monomer conversion.

The EVA copolymerization reaction is exothermic and temperature distribution in the reactor is closely related to the mixing. The reaction zone between the inlet 4 and the outlet was selected to investigate the influence of impeller speed on temperature distribution. Fig. 8(a) shows the maximum temperature difference of the reactor cross-sections at different heights (z/H=0-0.26). The stream from inlet 4 cooled the fluid near the wall, while the fluid near the stirring shaft was not well mixed with the cold stream and still maintained a high temperature. Therefore, the maximum temperature difference of the cross-sections near inlet 4 was large. As the reaction progressed, the cold stream was gradually heated and the maximum temperature difference of each cross-section decreased along the axial direction. As the impeller speed increased, the maximum temperature difference of each cross-section gradually decreased, which was attributed to the improved mixing. When the impeller speed increased to 700 rpm and 900 rpm, the maximum temperature difference of each cross-section dropped below 3 K. It indicates that the temperature distribution was uniform and the reactants were well mixed.

Fig. 8(b) is the curve of the specific initiator consumption per 1% of the monomer reacted (W_I) as a function of the impeller speed. As the impeller speed increased from 100 rpm to 900 rpm, W_I decreased from 0.0796 kg/h to 0.0623 kg/h. It indicates that poor mixing reduced the efficiency of the initiator. Increasing the impeller speed can improve the mixing, thereby increasing the efficiency of the initiator.

Fig. 8(c) shows the effects of the impeller speed on the stirring power consumption per unit reactor volume (P_V) and the outlet monomer conversion. P_V obtained according to the formula (31) [31]:

$$P_V = \frac{2\pi N M_T}{60V} \tag{31}$$

in which, N is the impeller speed, M_T is the stirring torque, and V is the reactor volume.

As the impeller speed increased from 100 rpm to 700 rpm, the monomer conversion increased from 12.3% to 15.5%. It was attri-

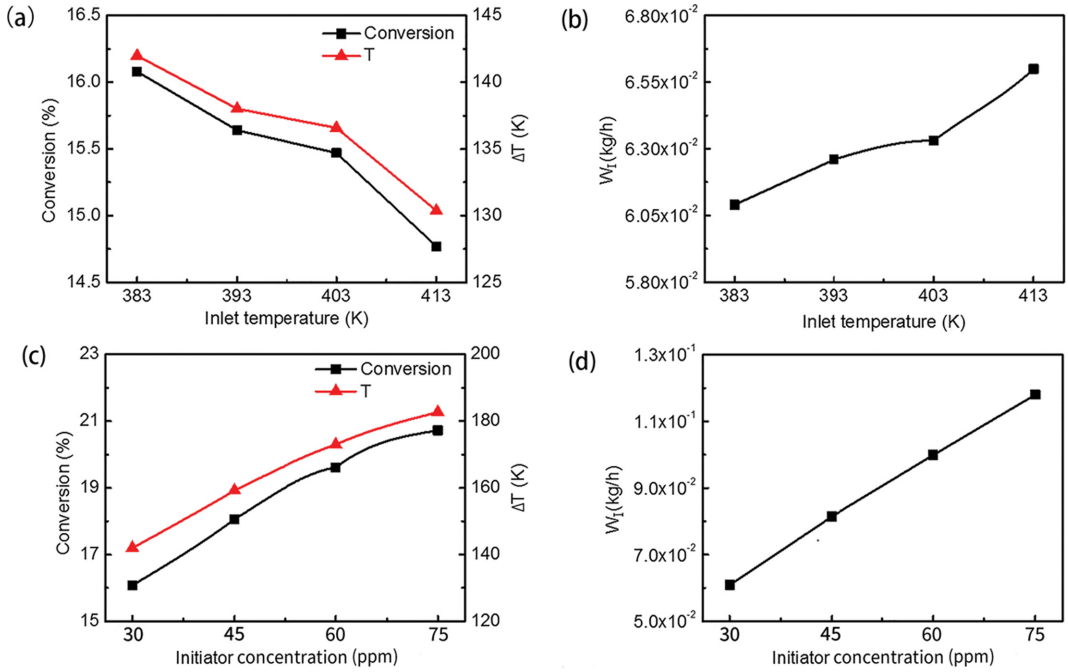

Fig. 9. The effects of inlet temperature on (a) monomer conversion and ΔT, (b) W_I; and the effects of initiator concentration on (c) monomer conversion and ΔT, (d) W_I.

buted to the improvement in mixing, which increased the reaction probability of monomers, initiators, and free radicals. Erdogan et al. [32] had observed the same phenomenon in styrene polymerization experiments. As the impeller speed increased from 700 rpm to 900 rpm, P_V was significantly increased, while the change of conversion was negligible. Therefore, the optimal impeller speed is 700 rpm.

4. Influence of Inlet Temperature and Initiator Concentration

The influence of inlet temperature on the EVA copolymerization process was investigated at a constant impeller speed of 700 rpm, initiator concentration of 30 ppm. Fig. 9(a) shows the effects of inlet temperature on monomer conversion and the temperature rise (ΔT) of the feeds at the outlet compared to the inlet. Since the reactor was adiabatic, the heat released by monomer polymerization increased the temperature of the outlet feed. It can be seen from Fig. 9(a) that the conversion and ΔT show the same trend of change. As the inlet temperature increased from 383 K to 413 K, the monomer conversion decreased from 16.08% to 14.77%. The decrease of monomer conversion was attributed to the increase of reaction temperature, which greatly increased the chain termination rate. The excessive termination of the active polymer chains made it difficult to initiate more monomers. Fig. 9(b) shows the variation of W_I with inlet temperature. As the inlet temperature increased from 383 K to 413 K, W_I increased from 0.0619 kg/h to 0.0664 kg/h. It shows that within the investigated inlet temperature range, a higher inlet temperature is not conducive to the efficient use of the initiator. Due to the higher decomposition temperature of the initiator used in this study, we used higher inlet temperatures in the simulation. Note that in industrial autoclaves, a mixture of initiators with different half-lives is commonly used and the inlet temperature can be controlled below 363 K.

The influence of initiator concentration on EVA copolymerization process was investigated at a constant impeller speed of 700 rpm and inlet temperature of 383 K. Fig. 9(c) shows that as the initiator concentration increased from 30 ppm to 75 ppm, the monomer conversion increased from 16.08% to 20.72%, and ΔT increased from 142 K to 183 K. More primary free radicals were generated as the initiator concentration increased. The primary free radicals generated by the decomposition of the initiator increased with the increase of the initiator concentration, thereby initiating more monomers to participate in the polymerization. However, it can be seen from Fig. 9(d) that W_I greatly increased with the increase of the initiator concentration. Therefore, it is necessary to consider both the initiator's conversion and utilization efficiency when selecting the initiator concentration.

CONCLUSION

A full-scale industrial EVA autoclave reactor model was established by combining computational fluid dynamics (CFD) with polymerization kinetics. The established model well predicts the detailed flow field distribution of the reactor, which can provide the basis for the reactor and impeller design. The conversion and initiator consumption are closely related to the flow characteristics in the reactor, and the established model can guide the optimization of process conditions. In addition, accurate prediction of the temperature field is achieved by coupling the reaction kinetics, which can be used to guide the design of the reactor to avoid temperature runaway.

As the speed of the impeller increases, the flow pattern changes and the axial and radial flow increases. The increase of impeller speed is beneficial to increasing the conversion and decreasing the

initiator consumption per 1% of monomer reacted (W_I). Increasing the inlet temperature will reduce the monomer conversion and W_I in the investigated temperature range. Both conversion and W_I increased with increasing initiator concentration. Our research results have guiding significance for the design and operation of industrial EVA autoclave reactors.

This paper only considers the effect of operating conditions on the conversion and initiator consumption. The research on crucial product parameters such as molecular weight distribution will be carried out in the future works to provide a reference for the regulation of EVA product grades.

NOMENCLATURE

A : modifier
$D_{m,i}$: diffusion coefficient of component m [$m^2 \cdot s^{-1}$]
E_a : activation energy [$J \cdot mol^{-1} \cdot K^{-1}$]
e : total energy [$J \cdot kg^{-1}$]
f : apparent initiator efficiency factor
h : specific enthalpy [$J \cdot kg^{-1}$]
$J_{m,i}$: diffusion flux of component m [$kg \cdot m^{-2} \cdot s^{-1}$]
k : turbulent kinetic energy [$J \cdot kg^{-1} \cdot s^{-1}$]
k_0 : frequency factor [s^{-1} or $L \cdot mol^{-1} \cdot s^{-1}$]
k_d : initiator decomposition rate coefficient [$L \cdot s^{-1}$]
k_{eff} : effective thermal conductivity [$W \cdot m^{-1} \cdot K^{-1}$]
k_{in} : initiation rate coefficient [$L \cdot mol^{-1} \cdot s^{-1}$]
k_p : propagation rate coefficient [$L \cdot mol^{-1} \cdot s^{-1}$]
k_{ta} : chain transfer to modifier rate coefficient [$L \cdot mol^{-1} \cdot s^{-1}$]
k_{tc} : termination by combination rate coefficient [$L \cdot mol^{-1} \cdot s^{-1}$]
k_{td} : termination by disproportionation rate coefficient [$L \cdot mol^{-1} \cdot s^{-1}$]
k_{tm} : chain transfer to monomer rate coefficient [$L \cdot mol^{-1} \cdot s^{-1}$]
k_{tp} : chain transfer to polymer rate coefficient [$L \cdot mol^{-1} \cdot s^{-1}$]
k_β : β-scission of internal radicals rate coefficient [$L \cdot mol^{-1} \cdot s^{-1}$]
M_T : stirring torque [N·m]
N : impeller speed [rpm]
P_V : impeller power consumption per unit volume [$W \cdot m^{-3}$]
p : pressure [Pa]
r : reaction rate [$mol \cdot L^{-1} \cdot s^{-1}$]
S_h : heat source term due to polymerization [$J \cdot m^{-3} \cdot s^{-1}$]
S_i : reaction source of component i [$J \cdot m^{-3} \cdot s^{-1}$]
Sc_t : Schmidt number
T : temperature [K]
u_i : velocity components [$m \cdot s^{-1}$]
V : reactor volume [m^3]
W_I : the specific initiator consumption per 1% of the monomer reacted [$kg \cdot h^{-1}$]
Y_m : mass fraction of component m

Greek Letters

ΔT : the outlet temperature rise [K]
ΔV : activation volume [$cm^3 \cdot mol^{-1}$]
δ_{ij} : Kronecker delta
ε : Turbulent kinetic energy dissipation rate [$J \cdot kg^{-1} \cdot s^{-1}$]
λ_i : moment of the live polymer chains [$mol \cdot L^{-1}$]
μ_i : moment of the dead polymer chains [$mol \cdot L^{-1}$]
μ : dynamic viscosity [Pa·s]
μ_t : turbulent viscosity [Pa·s]
ρ : mixture density [$kg \cdot m^{-3}$]
τ_{ij} : stress tensor [Pa]

Subscripts

d : initiation decomposition
in : initiator
m : chain length
n : chain length
p : propagation
ta : chain transfer to modifier
tc : termination by combination
td : termination by disproportionation
tm : chain transfer to monomer
tp : chain transfer to polymer
z : chain length
β : β-scission of internal radicals

SUPPORTING INFORMATION

Additional information as noted in the text. This information is available via the Internet at http://www.springer.com/chemistry/journal/11814.

REFERENCES

1. S. P. Tambe, S. K. Singh, M. Patri and D. Kumar, *Prog. Org. Coat.*, **62**, 382 (2008).
2. A. Zarrouki, E. Espinosa, C. Boisson and V. Monteil, *Macromolecules*, **50**, 3516 (2017).
3. M. Ghiass and R. A. Hutchinson, *Polym. React. Eng.*, **11**, 989 (2003).
4. G. J. Wells and W. H. Ray, *AIChE J.*, **51**, 3205 (2005).
5. P. Pladis and C. A. Kiparissides, *Ind. Eng. Chem. Res.*, **58**, 13093 (2019).
6. C. Kiparissides, G. Verros and J. A. Macgregor, *J. Macromol. Sci., Polym. Rev.*, **33**, 437 (1993).
7. Y. Lee, K. Jeon, J. Cho, J. Na, J. Park, I. Jung, J. Park, M. J. Park and W. B. Lee, *Ind. Eng. Chem. Res.*, **58**, 16459 (2019).
8. H. Patel, R. Dhib and F. Ein-Mozaffari, *Chem. Eng. Technol.*, **33**, 258 (2010).
9. S. F. Roudsari, F. Ein-Mozaffari and R. Dhib, *Chem. Eng. J.*, **219**, 429 (2013).
10. C. Xu, J. Wang, X. Gu and L. Feng, *Chem. Eng. Commun.*, **205**, 857 (2018).
11. G. J. Wells and W. H. Ray, *Macromol. Mater. Eng.*, **290**, 319 (2005).
12. G. Luft, M. Jabbari and M. Dorn, *Angew. Makromol. Chem.*, **238**, 87 (1996).
13. I. L. Chien, T. W. Kan and B.-S. Chen, *Comput. Chem. Eng.*, **31**, 233 (2007).
14. N. Jacob and R. Dhib, *J. Ind. Eng. Chem.*, **18**, 1781 (2012).
15. C. Sarmoria, A. Brandolin, A. Lopez-Rodriguez, K. S. Whiteley and B. D. Fernandez, *Polym. Eng. Sci.*, **40**, 1480 (2000).
16. J. Cui, L. Ni, J. Jiang, Y. Pan, H. Wu and Q. Chen, *Org. Process Res. Dev.*, **23**, 389 (2019).
17. N. K. Read, S. X. Zhang and W. H. Ray, *AIChE J.*, **43**, 104 (1997).

18. G. D. Wehinger, T. Eppinger and M. Kraume, *Chem. Eng. Sci.*, **122**, 197 (2015).
19. Y. Zhuang, X. Gao, Y. Zhu and Z. Luo, *Powder Technol.*, **221**, 419 (2012).
20. T. Shin, W. W. Liou, A. Shabbir, Z. Yang and J. Zhu, *Comput. Fluids*, **24**, 227 (1995)
21. P. Becker, M. Buback and J. Sandmann, *Macromol. Chem. Phys.*, **203**, 2113 (2002).
22. T. Xie and A. Hamielec, *Macromol. Theory Simul.*, **2**, 777 (1993).
23. T. Xie and A. Hamielec, *Macromol. Theory Simul.*, **2**, 455 (1993).
24. T. Xie and A. Hamielec, *Macromol. Theory Simul.*, **2**, 421 (1993).
25. A. Hamielec, J. MacGregor and A. Penlidis, *Makromolekulare Chemie. Macromol. Symp.*, **10-11**, 521 (1987).
26. J. Soares, *Chem. Eng. Sci.*, **56**, 4131 (2001).
27. P. Pladis and C. Kiparissides, *Chem. Eng. Sci.*, **53**, 3315 (1998).
28. H. Hulburt and S. Katz, *Chem. Eng. Sci.*, **19**, 555 (1964).
29. S. Roudsari, G. Turcotte, R. Dhib and F. Ein-Mozaffari, *Comput. Chem. Eng.*, **45**, 124 (2012).
30. S. Zhang and W. Ray, *AIChE J.*, **43**, 1265 (1997).
31. C. He, J. Wang, R. Wang and X. Zhang, *Renew. Energ.*, **168**, 1177 (2021).
32. S. Erdogan, M. Alpbaz and A. R. Karagöz, *Chem. Eng. J.*, **86**, 259 (2002).

Supporting Information

Investigation on flow characteristic and reaction process inside an EVA autoclave reactor using CFD modeling combined with polymerization kinetics

Yiduo Wang*,, Cheng Liu*,**, Sheng Wang*,**, and He Dong*,**,†**

*Key Laboratory for Green Chemical Technology of the Ministry of Education, Tianjin University R&D Center for Petrochemical Technology, Tianjin 300072, China
**Collaborative Innovation Center of Chemical Science and Engineering, Tianjin 300072, China
(*Received 15 October 2021 • Revised 20 January 2022 • Accepted 23 January 2022*)

Derivation of rate functions for the moments of the number of chain length distributions of the 'live' and 'dead' polymer chains:

The elementary reactions considered in this study include initiator decomposition, initiation, propagation, chain transfer to monomer, chain transfer to polymer, chain transfer to the modifier, termination by combination, termination by disproportionation, and β-scission of internal radicals [6,8]. In order to simplify the calculation of the copolymerization reaction, Xie et al. [9-11] proposed the pseudo-kinetic rate constant method. The elementary reactions and the pseudo-kinetic rate constants of the ethylene-VA binary copolymerization are shown in Table S1.

f_i is the mole fraction of monomer *i* in monomer mixture,

$$f_1=\frac{M_1}{M_1+M_2} \tag{1}$$

$$f_2=1-f_1 \tag{2}$$

φ_i is the mole fraction of radical *i*, which can be derived from the assumption of the long chain approximation [12,13],

$$k_{pij}\varphi_i f_j=k_{pji}\varphi_j f_i \tag{3}$$

$$\varphi_1=\frac{k_{p21}f_1}{k_{p21}f_1+k_{p12}f_2} \tag{4}$$

$$\varphi_2=1-\varphi_1 \tag{5}$$

F_i is the mole fraction of monomer *i* in polymer [6],

$$F_1=\frac{(r_1-1)f_1^2+f_1}{(r_1+r_2-2)f_1^2+2(1-r_2)f_1+r_2} \tag{6}$$

$$F_2=1-F_1 \tag{7}$$

where r_1, r_2 are reactivity ratios.

According to the elementary reaction, the rate equation of each species can be derived:

Table S1. EVA copolymerization reaction mechanism and pseudo-kinetic rate constants

Elementary reaction	Mechanism	Pseudo-kinetic rate constants
Initiator decomposition	$I_l \xrightarrow{k_{dl}} 2R_0 (l=1, 2 \ldots N_I)$	
Initiation	$R_0+M \xrightarrow{k_{in}} R_1$	$k_{in}=\sum_{j=1}^{2}k_{inj}f_j$
Propagation	$R_n+M \xrightarrow{k_p} R_{n+1}$	$k_p=\sum_{i=1}^{2}\sum_{j=1}^{2}k_{pij}\varphi_i f_j$
Termination by combination	$R_m+R_n \xrightarrow{k_{tc}} P_{m+n}$	$k_{tc}=\sum_{i=1}^{2}\sum_{j=1}^{2}k_{tcij}\varphi_i\varphi_j$
Termination by disproportionation	$R_m+R_n \xrightarrow{k_{td}} P_m+P_n$	$k_{td}=\sum_{i=1}^{2}\sum_{j=1}^{2}k_{tdij}\varphi_i\varphi_j$
Chain transfer to monomer	$R_n+M \xrightarrow{k_{tm}} R_1+P_n$	$k_{tm}=\sum_{i=1}^{2}\sum_{j=1}^{2}k_{tmij}\varphi_i f_j$
Chain transfer to polymer	$R_n+P_m \xrightarrow{k_{tp}} R_m+P_n$	$k_{tp}=\sum_{i=1}^{2}\sum_{j=1}^{2}k_{tpij}\varphi_i F_j$
Chain transfer to modifier	$R_n+A \xrightarrow{k_{ta}} R_1+P_n$	$k_{ta}=\sum_{j=1}^{2}k_{tai}\varphi_i$
β-scission of internal radicals	$R_n+P_m \xrightarrow{k_\beta} R_z+P_n+P_{m-z}$	$k_\beta=\sum_{i=1}^{2}\sum_{j=1}^{2}k_{\beta ij}\varphi_i F_j$

$$r_{I_i} = -k_{di}[I_i] \quad (i=1, 2 \ldots N_I) \tag{8}$$

$$r_M = -k_i[R_0][M] - k_p[M]\sum_{n=1}^{\infty}[R_n] - k_{trm}[M]\sum_{n=1}^{\infty}[R_n] \tag{9}$$

$$r_A = -k_{ta}[A]\sum_{n=1}^{\infty}[R_n] \tag{10}$$

$$r_{R_0} = \sum_{i=1}^{N_I} 2f_i k_{di}[I_i] - k_i[R_0][M] \tag{11}$$

$$\begin{aligned} r_{R_1} = {} & k_i[R_0][M] - k_p[R_1][M] + (k_{tm}[M] + k_{ta}[A])\sum_{n=1}^{\infty}[R_n] \\ & - k_{tp}[R_1]\sum_{n=2}^{\infty} n[P_n] - k_{tc}[R_1]\sum_{n=1}^{\infty}[R_n] \\ & - k_\beta[R_1]\sum_{n=2}^{\infty} n[P_n] + k_\beta\sum_{n=1}^{\infty}[R_n]\sum_{m=2}^{\infty}[P_m] \end{aligned} \tag{12}$$

$$\begin{aligned} r_{R_n} = {} & k_p([R_{n-1}] - [R_n])[M] - (k_{tm}[M] + k_{ta}[A])[R_n] + k_{tp} n[P_n]\sum_{n=1}^{\infty}[R_n] \\ & - k_{tp}[R_n]\sum_{n=2}^{\infty} n[P_n] - k_{tc}[R_n]\sum_{n=1}^{\infty}[R_n] - k_{td}[R_n]\sum_{n=1}^{\infty}[R_n] \\ & - k_\beta[R_n]\sum_{n=2}^{\infty} n[P_n] + k_\beta\sum_{n=1}^{\infty}[R_n]\sum_{m=n+1}^{\infty}[P_m] \end{aligned} \tag{13}$$

$$\begin{aligned} r_{P_n} = {} & (k_{tm}[M] + k_{ta}[A])[R_n] + k_{td}[R_n]\sum_{n=1}^{\infty}[R_n] + \frac{1}{2}k_{tc}\sum_{m=1}^{\infty}[R_m][R_{m-n}] \\ & + k_{tp}[R_n]\sum_{n=2}^{\infty} n[P_n] - k_{tp} n[P_n]\sum_{n=1}^{\infty}[R_n] + k_\beta[R_n]\sum_{n=2}^{\infty} n[P_n] \\ & + k_\beta\sum_{n=1}^{\infty}[R_n]\sum_{m=n+1}^{\infty}[P_m] - k_\beta n[P_n]\sum_{n=1}^{\infty}[R_n] \end{aligned} \tag{14}$$

Since the active polymer chain and the dead polymer chain have an infinite number of chain lengths, the moment method is used to simplify the differential equations to calculate the copolymer chain length distributions [5,6,14].

The zero moment, first moment, and second moment equations of the active polymer chain are as follows:

$$\lambda_i = \sum_{n=1}^{\infty} n^i[R_n] \tag{15}$$

The zero moment, first moment, and second moment equations of the dead polymer chain are as follows:

$$\mu_i = \sum_{n=2}^{\infty} n^i[P_n] \tag{16}$$

The corresponding rate functions for the moments of the number of chain length distributions of the 'live' and 'dead' polymer chains can be obtained by multiplying each term of Eqs. (12), (13), and (14) by term n^i and summing up the resulting expression over the total variation of n.

Here we provide the detailed derivation process of r_{λ_0} as an example:

$$\begin{aligned} r_{\lambda_0} = r_{\sum_{n=1}^{\infty}[R_n]} = {} & \sum_{n=1}^{\infty} r_{[R_n]} = r_{[R_1]} + r_{[R_2]} + \cdots r_{[R_n]} \\ = {} & \Big\{ k_i[R_0][M] - k_p[R_1][M] + (k_{tm}[M] + k_{ta}[A])\sum_{n=1}^{\infty}[R_n] \\ & - k_{tp}[R_1]\sum_{n=2}^{\infty} n[P_n] - k_{tc}[R_1]\sum_{n=1}^{\infty}[R_n] - k_{td}[R_1]\sum_{n=1}^{\infty}[R_n] \\ & - k_\beta[R_1]\sum_{n=2}^{\infty} n[P_n] + k_\beta\sum_{n=1}^{\infty}[R_n]\sum_{m=2}^{\infty}[P_m] \Big\} \\ & + \Big\{ k_p([R_1] - [R_2])[M] - (k_{tm}[M] + k_{ta}[A])[R_2] + k_{tp} 2[P_2]\sum_{n=1}^{\infty}[R_n] \\ & - k_{tp}[R_2]\sum_{n=2}^{\infty} n[P_n] - k_{tc}[R_2]\sum_{n=1}^{\infty}[R_n] - k_{td}[R_2]\sum_{n=1}^{\infty}[R_n] \\ & - k_\beta[R_2]\sum_{n=2}^{\infty} n[P_n] + k_\beta\sum_{n=1}^{\infty}[R_n]\sum_{m=n+1}^{\infty}[P_m] \Big\} + \cdots \\ & + \Big\{ k_p([R_{n-1}] - [R_n])[M] - (k_{tm}[M] + k_{ta}[A])[R_n] + k_{tp} n[P_n]\sum_{n=1}^{\infty}[R_n] \\ & - k_{tp}[R_n]\sum_{n=2}^{\infty} n[P_n] - k_{tc}[R_n]\sum_{n=1}^{\infty}[R_n] - k_{td}[R_n]\sum_{n=1}^{\infty}[R_n] \\ & - k_\beta[R_n]\sum_{n=2}^{\infty} n[P_n] + k_\beta\sum_{n=1}^{\infty}[R_n]\sum_{m=n+1}^{\infty}[P_m] \Big\} \\ = {} & k_i[R_0][M] + k_p\sum_{n=1}^{\infty}[R_n][M] - k_p\sum_{n=1}^{\infty}[R_n][M] \\ & + (k_{tm}[M] + k_{ta}[A])\sum_{n=1}^{\infty}[R_n] + k_{tp}\sum_{n=1}^{\infty}[R_n]\sum_{n=2}^{\infty} n[P_n] \\ & - k_{tp}\sum_{n=1}^{\infty}[R_n]\sum_{n=2}^{\infty} n[P_n] - (k_{tm}[M] + k_{ta}[A])\sum_{n=1}^{\infty}[R_n] \\ & - (k_{tc} + k_{td})\sum_{n=1}^{\infty}[R_n]\sum_{n=1}^{\infty}[R_n] - k_\beta\sum_{n=1}^{\infty}[R_n]\sum_{n=2}^{\infty} n[R_n] \\ & + k_\beta\sum_{n=1}^{\infty}[R_n]\sum_{n=2}^{\infty} n[R_n] = k_i[R_0][M] - (k_{tc} + k_{td})\lambda_0^2 \end{aligned}$$

Since the initiation rate is much greater than the initiator decomposition rate, the R_0 generated by the initiator decomposition can quickly react with the monomer to generate R_1, so it can be considered that

$$\sum_{i=1}^{N_I} 2f_i k_{di}[I_i] = k_i[R_0][M] \tag{17}$$

$$r_{\lambda_0} = \sum_{i=1}^{N_I} 2f_i k_{di}[I_i] - (k_{tc} + k_{td})\lambda_0^2 \tag{18}$$

Since only one initiator is considered in this study, r_{λ_0} can be expressed as

$$r_{\lambda_0} = 2fk_d[I] - (k_{tc} + k_{td})\lambda_0^2 \tag{19}$$

r_{λ_1}, r_{λ_2}, r_{μ_0}, r_{μ_1}, and r_{μ_2} are derived in the same way as r_{λ_0}. The final moment rate equations are:

$$r_{\lambda_0} = 2fk_d[I] - (k_{tc} + k_{td})\lambda_0^2 \tag{20}$$

$$\begin{aligned} r_{\lambda_1} = {} & 2fk_d[I] - (k_{tm}[M] + k_{ta}[A])\lambda_1 + k_p[M]\lambda_0 + k_{tp}(\mu_2\lambda_0 - \mu_1\lambda_1) \\ & - (k_{tc} + k_{td})\lambda_0\lambda_1 + k_\beta\left(\frac{1}{2}\mu_2\lambda_0 - \mu_1\lambda_1\right) \end{aligned} \tag{21}$$

$$\begin{aligned} r_{\lambda_2} = {} & 2fk_d[I] - (k_{tm}[M] + k_{ta}[A])\lambda_2 + 2k_p[M]\lambda_1 + k_{tp}(\mu_3\lambda_0 - \mu_1\lambda_2) \\ & - (k_{tc} + k_{td})\lambda_0\lambda_2 + k_\beta\left(\frac{1}{3}\mu_3\lambda_0 - \frac{1}{2}\mu_2\lambda_0 + \frac{1}{6}\mu_1\lambda_0 - \mu_1\lambda_2\right) \end{aligned} \tag{22}$$

$$r_{\mu_0} = (k_{tm}[M] + k_{ta}[A])\lambda_0 + \left(\frac{1}{2}k_{tc} + k_{td}\right)\lambda_0^2 + k_\beta\lambda_0\mu_1 \tag{23}$$

$$\begin{aligned} r_{\mu_1} = {} & (k_{tm}[M] + k_{ta}[A])\lambda_1 - k_{tp}(\mu_2\lambda_0 - \mu_1\lambda_1) + (k_{td} + k_{tc})\lambda_0\lambda_1 \\ & + k_\beta\left(\lambda_1\mu_1 - \frac{1}{2}\lambda_0\mu_0\right) \end{aligned} \tag{24}$$

$$r_{\mu_2} = (k_{tm}[M] + k_{ta}[A])\lambda_2 - k_{tp}(\mu_3\lambda_0 - \mu_1\lambda_2) + (k_{td} + k_{tc})\lambda_0\lambda_2 + k_{tc}\lambda_1^2 + k_{\beta}\left[\lambda_2\mu_2 - \lambda_0\left(\frac{2}{3}\mu_3 + \frac{1}{2}\mu_2 - \frac{1}{6}\mu_1\right)\right] \quad (25)$$

When transfer to polymer reactions are included in the kinetic mechanism, the n-order polymer moment equation will depend on the (n+1)-order moment. The Hulburt and Katz approximation [15] was employed to break down this moment dependence in the present study. This technique assumes that the molecular weight distribution can be represented by a truncated (after the first term) series of Laguerre polynomials by using a gamma distribution weighting function. Assuming that the first three terms of the Laguerre polynomials are sufficient for the representation of the molecular weight distribution, it can be shown that the third moment of the number chain length distribution can be expressed as:

$$\mu_3 = \frac{\mu_2}{\mu_1\mu_0}(2\mu_2\mu_0 - \mu_1^2) \quad (26)$$

The above closure method was applied to each polymer class of the 'dead' polymer chains.

REFERENCES

1. M. Ghiass and R. A. Hutchinson, *Polym. React. Eng.*, **11**, 989 (2003).
2. N. K. Read, S. X. Zhang and W. H. Ray, *AIChE J.*, **43**, 104 (1997).
3. T. Xie and A. Hamielec, *Macromol. Theory Simul.*, **2**, 777 (1993).
4. T. Xie and A. Hamielec, *Macromol. Theory Simul.*, **2**, 455 (1993).
5. T. Xie and A. Hamielec, *Macromol. Theory Simul.*, **2**, 421 (1993).
6. A. Hamielec, J. MacGregor and A. Penlidis, *Makromolekulare Chemie. Macromol. Symp.*, **10-11**, 521 (1987).
7. J. Soares, *Chem. Eng. Sci.*, **56**, 4131 (2001).
8. P. Pladis and C. Kiparissides, *Chem. Eng. Sci.*, **53**, 3315 (1998).
9. Y. Lee, K. Jeon, J. Cho, J. Na, J. Park, I. Jung, J. Park, M. J. Park and W. B. Lee, *Ind. Eng. Chem. Res.*, **58**, 16459 (2019).
10. H. Hulburt and S. Katz, *Chem. Eng. Sci.*, **19**, 555 (1964).